[PS]Integration of Imaging Techniques over Multiple Scales*

Samuel T. Best[1], Stephen O. Sears[2], and Clinton S. Willson[1]

Search and Discovery Article #40568 (2010)
Posted December 31, 2010

*Adapted from poster presentation at AAPG International Conference and Exhibition, Calgary, Alberta, Canada, September 12-15, 2010

[1]Department of Civil and Environmental Engineering, Louisiana State University (sbest1@tigers.lsu.edu)
[2]Craft and Hawkins Department of Petroleum Engineering, Louisiana State University

Abstract

Generation of 3-D pore network models based on high-resolution X-ray computed tomography (XCT) is becoming increasingly popular for simulating pore-scale processes and phenomena within porous media. Pore network modeling is a very useful tool in fields such as chemical, petroleum engineering and hydrology and has proven valuable in modeling and understanding a variety of pore-scale processes and phenomena such as multiphase fluid distribution, fluid flow, solute transport and mixing, colloidal transport and deposition, and chemical reactions. One of the most vital components of pore-network modeling is the generation of a realistic representation of the pore structure within the media being studied. The accuracy of the image-based pore network structure can be highly influenced by the characteristic length scale of the pore structure and the image resolution due to the significance of pore connectivity and spatial correlations.

Methods such as using capillary pressure-saturation curves to estimate pore sizes, fitting measured pressure-saturation curves to curves generated by network models, and 3-D characterization using 2-D images have been used for generating the pore network structure of porous media systems. The first two methods, however, lack a uniqueness of the solution due to the dependency of their retention curves on both pore size distribution and topology of the pore space. Both methods also lack the ability to directly measure the connectivity of the pore space (i.e. provide information about each individual pore throat). 3-D reconstruction methods based on measured porosity and correlation of serial cross-sections exist, but depending on the isotropy, may lack the ability to accurately represent the 3-D pore network structure and preparation of 2-D cross-sections is a laborious and destructive technique. Assuming that the image resolution is sufficient to capture the length scales and connectivity, high-resolution XCT images can provide the basis for generating realistic models of pore network structures that are unique to the media of interest (e.g., Prodanovic et al., 2004; Al-Raoush and Willson, 2005).

The application of XCT for generating realistic pore-network structures also has its limitations. Most XCT systems today have resolutions up to approximately 1 μm, which is sufficient in capturing macroporosity (greater than about 2 μm) such as that between the crystalline grains of sandstones, but is not adequate for capturing microporosity (less than about 2 μm) such as that within authigenic clay in sandstones and micritized fossil fragments in carbonates. For some phenomena and processes (e.g. Darcy and non-Darcy single phase flow), this microporosity does not play a role in the primary fluid flow paths (Thompson et al., 2008); therefore, this scale of characterization may not be necessary. However, for processes such as multiphase flow where hydrocarbons may be diffusing from these micropores, solute transport, and flow in low permeability rocks, characterization or knowledge of the microporosity and fine-scale connectivity is crucial.

Here, we lay out a plan for augmenting XCT scan data, which can provide the foundation for solid/void (macroporosity) segmentation, with mineralogical data obtained using conventional core analyses such as thin section, SEM and mercury injection, with the ultimate goal of providing realistic 3D models of pore networks for modeling purposes. Here we focus primarily on the type and quality of the data that can be extracted from these techniques and demonstrate how they can be correlated.

Computed X-Ray Microtomography

XCT is a non-destructive and non-invasive imaging technique for investigating the internal structure of an object. In general, there are two types of XCT systems available, with pros and cons depending on the scope of the research. Industrial systems, which utilize polychromatic X-ray energies and have spatial resolutions ranging from 1 to several hundred μm, are ideal for viewing and characterizing large and dense samples and capturing macroscopic features (Ketcham and Carlson, 2001). Synchrotron-based XCT, which due to very high photon fluxes, can provide monochromatic X-rays allowing for element specific imaging and quantification (Al-Raoush and Willson, 2005). This feature can be extremely helpful for differentiating fluid phases or for qualitative identification of mineralogy. However, a major limitation of using a synchrotron X-ray source are the lower energies (typically <50 keV), which limit the sample size to a cm or two (Wildenschild et al., 2002). Regardless of the X-ray source, one major issue with the use of XCT is that the higher the resolution desired, the smaller the pixel size must become due to X-ray beam characteristics. This results in a reduction in the maximum field of view and may create concerns about the ability to image a representative elementary volume (REV) of the media at very high resolutions.

Traditional Petrographic and Petrophysical Analysis

Porosity determination from cores and conventional porosity logs (neutron, density, sonic) typically measure the total porosity in reservoir rocks, including microporosity which is often too small to contribute to fluid flow. Another common technique utilized to characterize the pore system is capillary pressure measurements using mercury, which provides a distribution of pore throat sizes. These petrophysical measurements are commonly used in conjunction with petrographic (thin section) and Scanning Electron

Microscope (SEM) analysis to create a three dimensional understanding of the pore networks. A diagram of the range in scales of characterization for each technique is presented in Figure 1. Pore sizes as small as 0.05 μm can be imaged with the SEM, and mercury injection can measure pore throats less than 0.005 μm, allowing an understanding of the total pore space in nearly all rock types. This approach also allows the distribution of microporosity to be tied to geologic processes such as the formation of authigenic clay in sandstones and the micritization of fossil fragments in carbonates. This data can also be used to estimate the distribution of pore throat sizes, which can be verified by comparison with mercury injection data. This combination of petrophysical, thin section, and SEM data has been used to predict permeability, water saturation, and other parameters in oil and gas reservoirs.

Approach

The approach of this study is to use traditional petrophysical and petrographic analysis to better understand and augment high-resolution XCT images and help make decisions concerning the accuracy and applicability of CMT images to network modeling. For this study, two 1 inch drill cores, one Indiana Limestone and one Castlegate Sandstone, were provided by ExxonMobil. 3 mm and 6 mm small cores were extracted in house from the 1 inch cores using diamond core drill bits. All imaging was performed at the X2B Beamline, National Synchrotron Light Source (NSLS), Brookhaven National Laboratory, Brookhaven, NY. The 3 mm Indiana Limestone and 6 mm Castlegate cores were imaged at resolutions/energies of 3.9 μm/28 keV and 7.6 μm/30 keV, respectively. Subvolumes of 1.170x1.170x1.268 (xyz) mm^3 (Indiana) and 2.271x2.271x3.217 (xyz) mm^3 (Castlegate) were extracted from the image files. The grayscale images were first processed using a nonlinear anisotropic diffusion program and then segmented to separate the solid and void phases using an indicator kriging-based program (Bhattad et al., 2010).

Petrophysical measurements including porosity, permeability, and mercury capillary injection measurements were performed by Weatherford Laboratories, Houston, TX. Porosity and permeability were measured at a confining stress of 5000 psi. Thin sections and SEM photographs were also provided by Weatherford and analyzed by the authors. Porosity values were estimated using a point count method on the thin section images.

The SEM and thin section images of the Indiana Limestone (Figure 2) show three distinct phases: non-porous fossil fragments filled and surrounded by secondary calcite cement, porous micrite with 2 μm diameter pore spaces between calcite grains, and void space (macroporosity) between cemented fossil fragments. These insights guided the segmentation of the Indiana Limestone in an effort to differentiate the three phases (Figure 3). The first segmentation of the grayscale Indiana XCT image (Figure 3a) separated the non-porous cemented fossil fragments and porous micrite (the two gray phases) from the void space (i.e., the black phase) identifying the macroporosity. The second segmentation separated the void space and the micrite (the dark gray phase) from the cemented fossil fragments. The two segmented images were then added together producing a three “phase” image with the black, gray and white regions denoting the macroporosity, micrite and cemented fossil fragments, respectively (Figure 3b). The “phase” volume fractions of the segmented XCT image were calculated directly by voxel counting.

The SEM and thin section images of the Castlegate Sandstone (Figure 4) also show three distinct phases: grains made up of primarily quartz and rock fragments, some authigenic clay containing microporosity, and void space. The authigenic clay (i.e. kaolinite clay) is located sandwiched between quartz grains and as coatings around the quartz grains. Following a similar procedure as described above, the grayscale Castlegate XCT image (Figure 5a) was segmented twice: first to separate the solid quartz and rock fragments (light gray) plus the authigenic clay (medium gray) from the void space; the second to separate the solid quartz and rock fragments from the authigenic clay plus the void space. The final segmented image (Figure 5b) shows the three regions: macroporosity, authigenic clay, and quartz and rock fragments in black, gray, and white, respectively. The porosity and "phase" volume fractions of the segmented XCT image were also calculated directly by voxel counting.

Results and Discussion

The point count on the thin section images of the Indiana Limestone determined a macroporosity of 10% and that the micrite contributed to 29% of the total volume. The micrite contains 2 μm size pores between 1-2 μm calcite crystals with an estimated microporosity of 25% of the total micrite volume. Therefore, the micrite contributes microporosity of 7% (0.29*0.25 = 0.07), which makes the total petrographically determined porosity 17%. The total petrophysically measured porosity is 15.2%, which is just slightly less than the point count estimation and within the +/- 6% error of the point count method. The XCT macroporosity calculated is 11.2%, only slightly higher than that estimated in the point count of the thin section and SEM. Segmentation of the XCT image yielded volume fractions of the XCT macroporosity (11.2%) and the micrite (35%). With a micrite porosity of 25% (from SEM) the overall microporosity of 9% within the sample; this results in a total porosity of 20%.

A point count of the Castlegate thin section gave the following details: 56% non-porous quartz grains, 18% non-porous rock fragments, 19% interparticle macroporosity, 1% intraparticle macroporosity, 1% secondary macroporosity, and 5% clay. SEM images of the clay show that about 40% of the clay is microporosity. The rock, therefore, has a total microporosity of approximately 2%. Weatherford Labs measured a total porosity of 25.1%, which is slightly higher than the total point count estimation of 23%. Existence of the kaolinite phase in the Castlegate grayscale XCT is not as distinct as the micrite phase in the Indiana due to similar clay and quartz X-ray absorption values. However, a third phase was noticeable as coatings around the quartz grains and sandwiched between grains (as seen in the SEM and thin section images). The first segmentation step resulted in a macroporosity of 18.5% which is very close to the point count estimation. After the second segmentation step, the kaolinite volume fraction was calculated to be 16.5%. The resulting microporosity is 6.6%, which is higher than the point count estimation of 2%. The XCT total porosity of the segmented image is 25.1%, the same as that provided by Weatherford labs.

Differences in micro- and macroporosity values from the XCT images compared to the corresponding point count values may be a result of either an over or under estimation of the micro- or macroporosities from the point counting, noise around the edges of the quartz grains in the XCT image, or that the SEM and thin sections are not representative of the XCT image. Addressing these issues is part of our current research.

Conclusion and Recommendations

Augmentation of XCT scan data with conventional core analysis can be a very useful tool to help understand the multi-scale pore network structure of many porous media types. SEM and thin section data can help differentiate between the macro and micro porosities of a system, which then can be incorporated into the segmentation process of XCT images. Three major limitations exist. The first is related to the X-ray absorption values and the ability to use XCT images to differentiate multiphase phases and materials. In this work, the Indiana grayscale XCT image clearly showed three distinguishable phases allowing for an easy 3-phase segmentation while the Castlegate grayscale XCT image did not as clearly show the different materials that were obvious in the SEM and thin section images. The second limitation, due to both spatial resolution and absorption differences, is clarity of the grayscale XCT and the sharpness of the edges resulting in less distinction between phases within the media making segmentation difficult. Finally, issues related to the representativeness and spatial distribution of the various materials need to be addressed so that the data and information obtained from these very fine scale techniques can be incorporated into macroscopic models that can be used for realistic predictions.

References

Al-Raoush, R.I. and C.S. Willson, 2005, Extraction of physically realistic pore network properties from three-dimensional synchrotron X-ray microtomography images of unconsolidated porous media systems: Journal of Hydrology, v. 300/1-4, p. 44-64.

Bhattad, P., C.S. Willson, and K.E. Thompson, 2010, Segmentation of low-contrast three-phase X-Ray computed tomography images of porous media: Proceedings of the GeoX 2010. 3rd International Workshop on X-ray CT for Geomaterials in New Orleans, LA, March 1-3, edited by K. Alshibli and A.H. Reed, p. 254-261.
http://www.cee.lsu.edu/geox2010/workshop/Program.html

Ketcham, R.A. and W.D. Carlson, 2001, Acquisition, optimization and interpretation of X-ray computed tomography imagery: applications to the geosciences, Computers and Geosciences, v. 27/4, p. 381-400.

Prodanovic, M., W.B. Lindquist, and R.S. Seright, 2005, 3D Image-Based Characterization of Fluid Displacement in a Berea Core: Advances in Water Resources, v. 30/2, p. 214-226.

Wildenschild, D., J.W. Hopmans, C.M.P. Vaz, M.L. Rivers, D. Rikard, and B.S.B. Christensen, 2002, Using X-ray computed tomography in hydrology: systems, resolutions, and limitations, Journal of Hydrology, v. 267/3-4, p. 285-297.

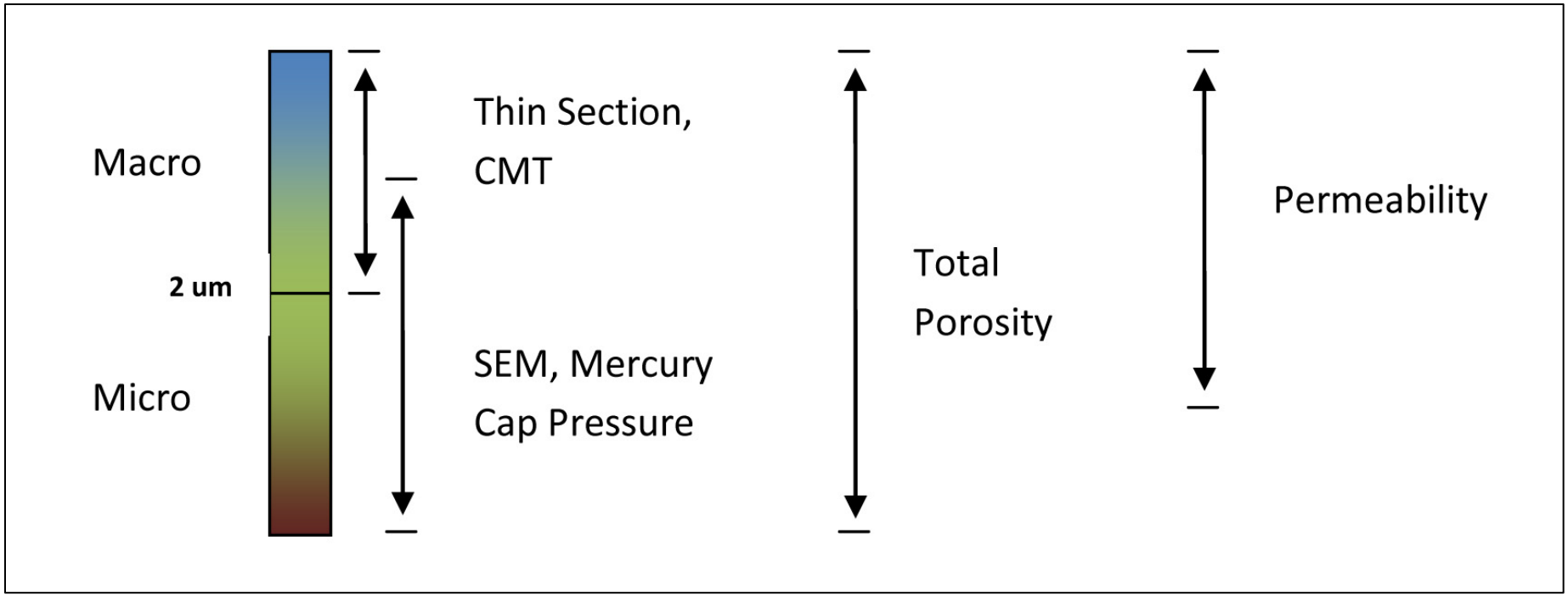

Figure 1. Porosity scales captured by various petrophysical and petrographic techniques.

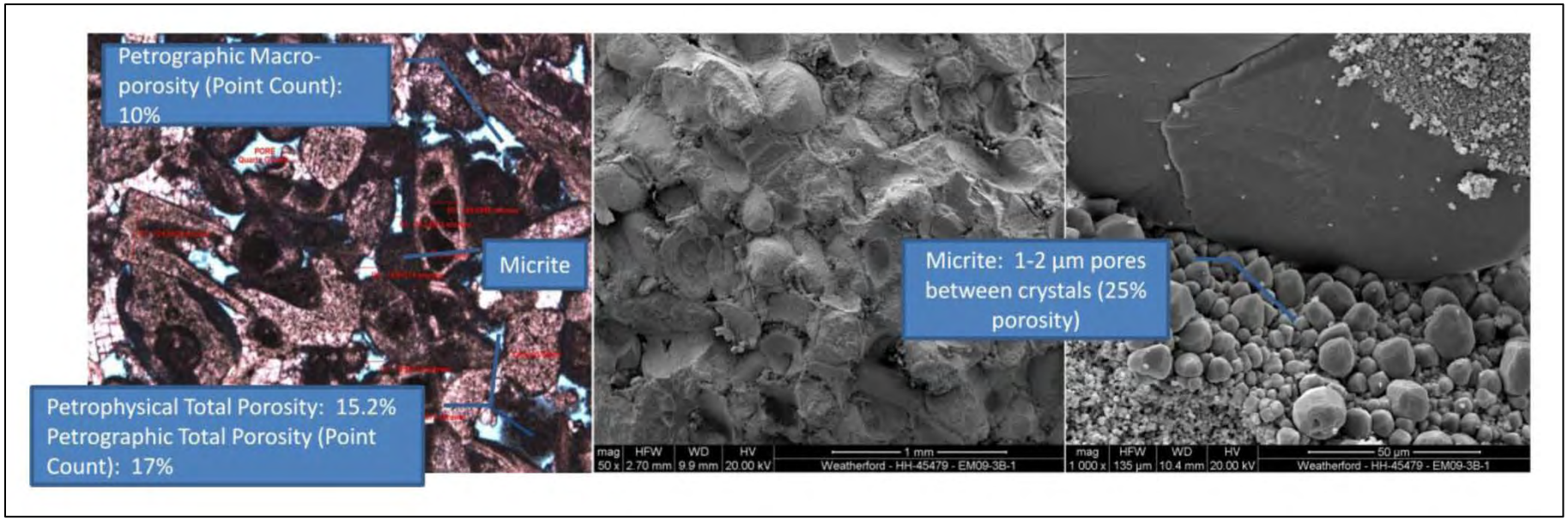

Figure 2. From left to right: (a) Plane Light 50X thin section, (b) 50X SEM, and (c) 1000X SEM.

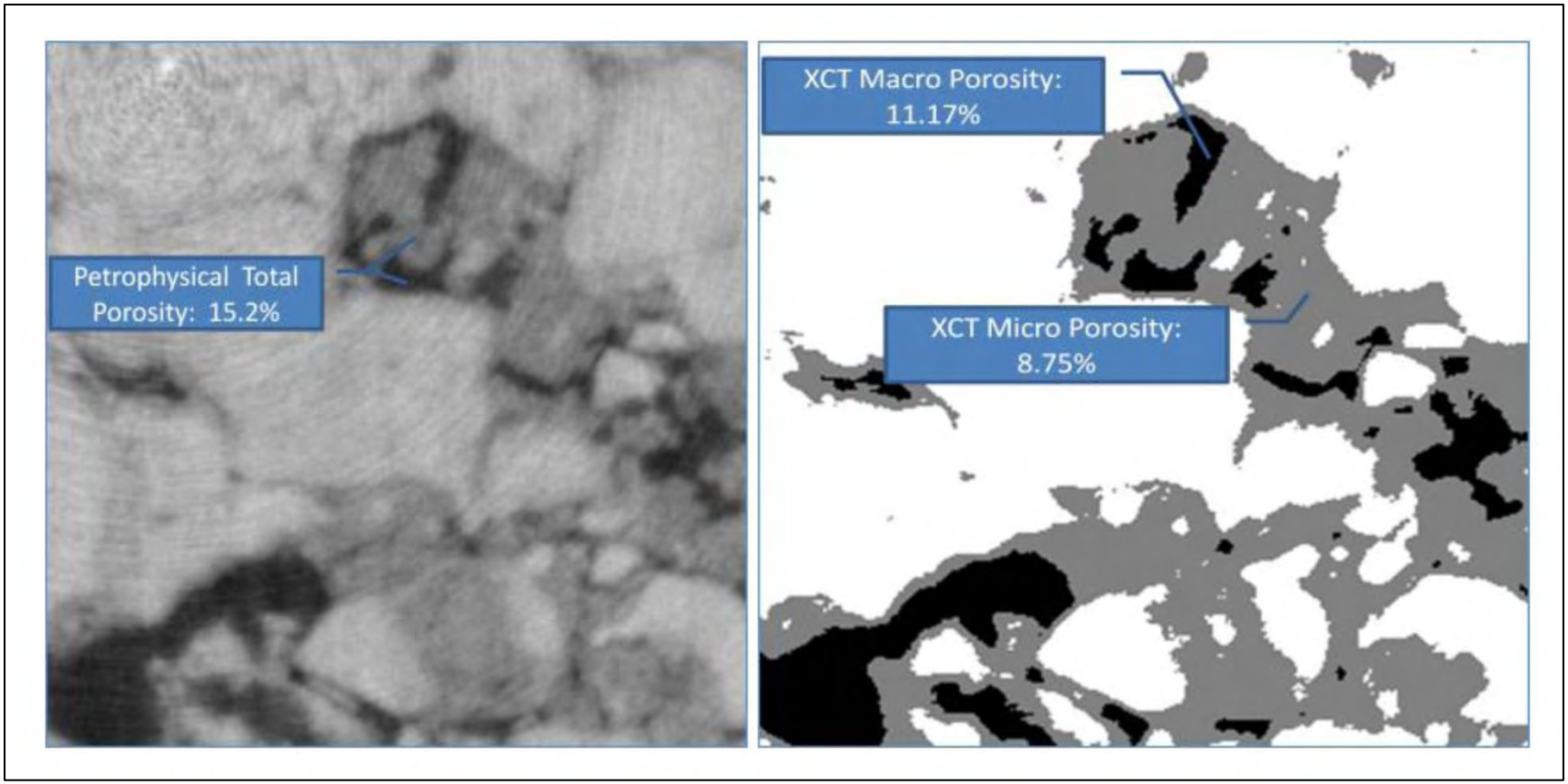

Figure 3. From left to right: (a) Original XCT image after noise reduction using anisotropic diffusion; (b) final 3-phase segmented image.

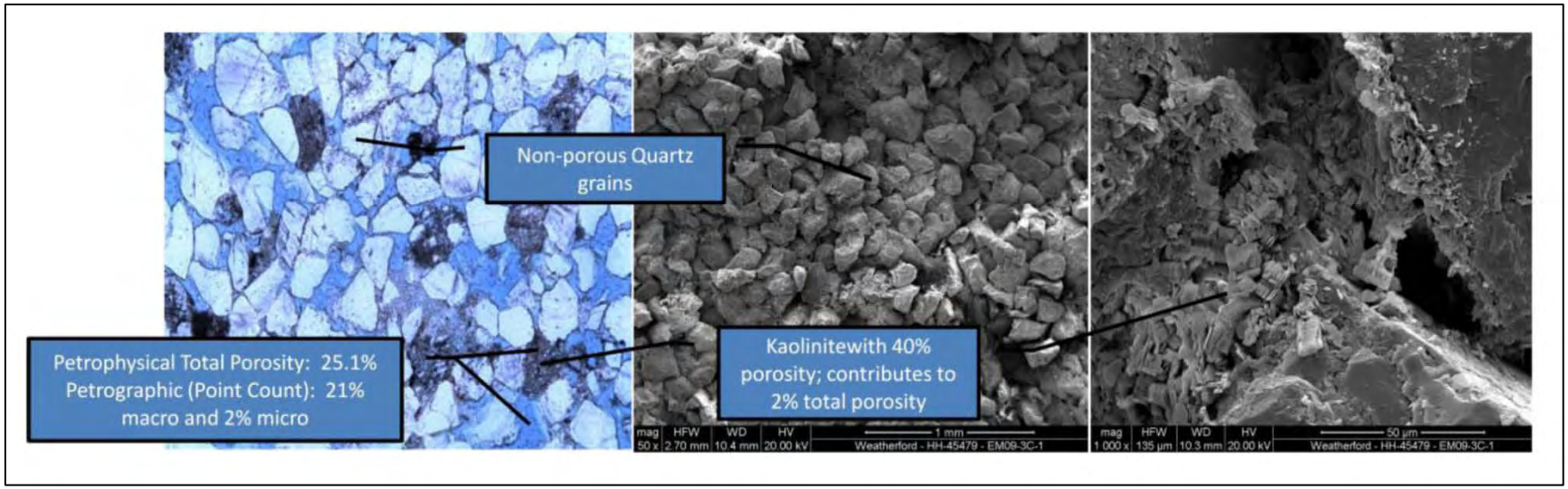

Figure 4. From left to right: (a) Plane Light 50X thin section, (b) 50X SEM, and (c) 1000X SEM.

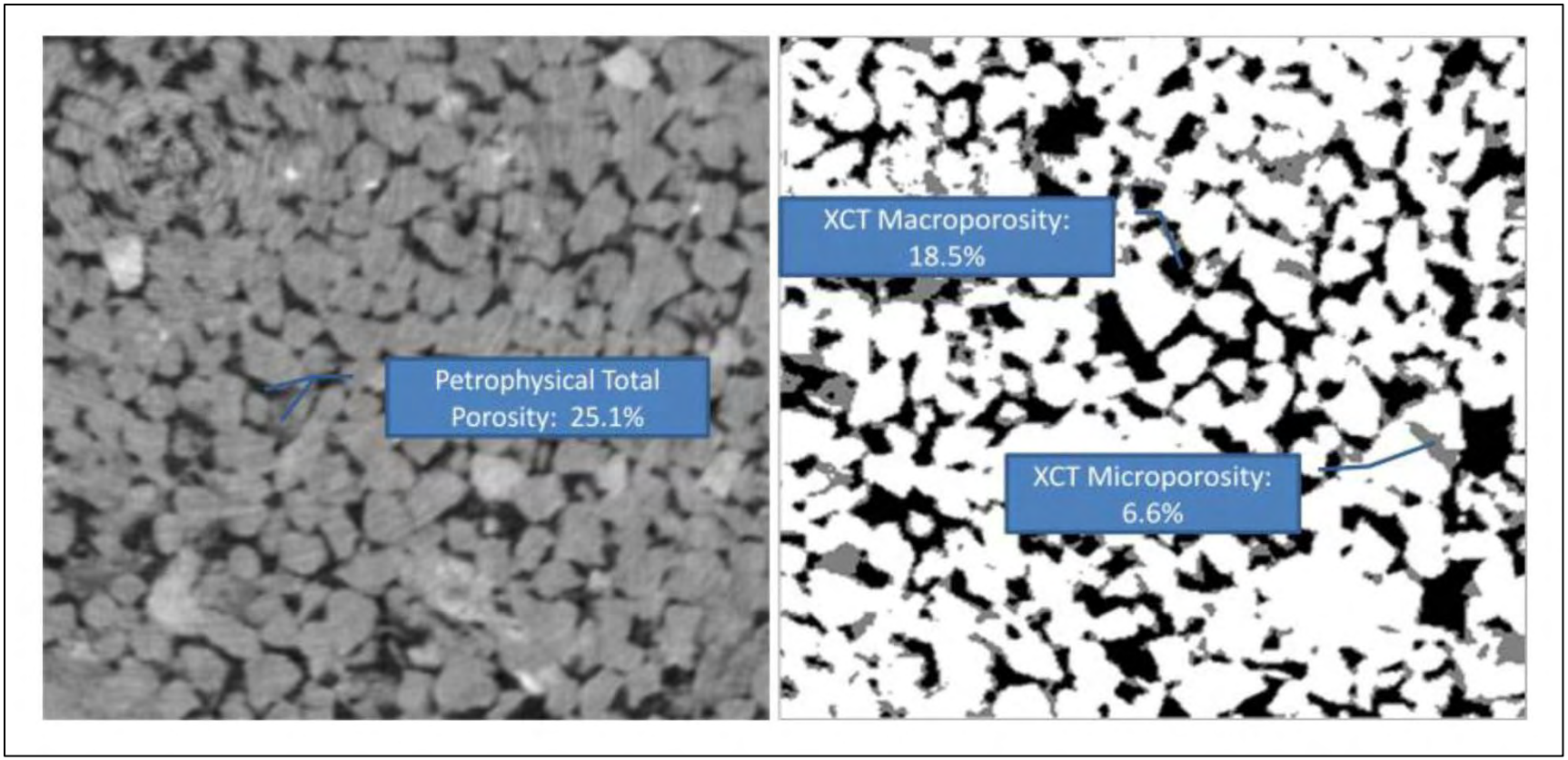

Figure 5. From left to right: (a) Original XCT image after noise reduction using anisotropic diffusion; (b) final 3-phase segmented image.